PROCEEDINGS, Thirty-Seventh Workshop on Geothermal Reservoir Engineering
Stanford University, Stanford, California, January 30 - February 1, 2012
SGP-TR-194

SUPERCRITICAL CO_2 IN A GRANITE-HOSTED GEOTHERMAL SYSTEM: EXPERIMENTAL INSIGHTS INTO MULTIPHASE FLUID-ROCK INTERACTIONS

Caroline Lo Ré[1], John Kaszuba[1, 2], Joseph Moore[3], Brian McPherson[3]

[1] University of Wyoming, Dept. of Geology & Geophysics, Laramie, WY 82071
[2] University of Wyoming, School of Energy Resources, Laramie, WY 82071
[3] University of Utah, Energy & Geoscience Institute, Salt Lake City, UT 84108
e-mail: flore@uwyo.edu

ABSTRACT

Geochemical modeling and hydrothermal experiments were conducted at 250°C and 25-45 MPa to evaluate associated geochemical and mineralogical relationships and to determine how geothermal systems may respond given 'spontaneous' injection of CO_2 into a granitic reservoir. Water + granite experiments reacted for ~28 days, and then two of the three systems were injected with supercritical CO_2 ($scCO_2$) and reacted for at least an additional 42 days. In addition to other minerals, the baseline water + granite experiment resulted in illite formation. The water + granite + $scCO_2$ experiments resulted in smectite formation. No carbonate minerals were observed as reaction products of these experiments. A baseline understanding of reactions involving a multi-component groundwater, a granite, and $scCO_2$ has been established. Results may improve our understanding of processes in natural and enhanced geothermal systems (EGS).

INTRODUCTION

In commercial geothermal operations, it is imperative that permeability and porosity not be reduced by chemical reactions instigated by working fluids, or at least that such changes in hydrologic properties be predictable and project design adjusted accordingly. A purpose of this study is to characterize some of the most likely chemical reactions that lead to these kinds of changes. Specifically, $scCO_2$ has recently been proposed as a working fluid in EGS due to its low viscosity, large expansivity, and reduced reactivity with rock as compared to water (Brown, 2000; Pruess, 2006). However, the interaction of $scCO_2$ with groundwater and host rock may induce dissolution/precipitation reactions as $scCO_2$-water mixtures migrate through the reservoir; unfavorable reductions of permeability and porosity may result. Geochemical modeling and hydrothermal experiments are underway to evaluate associated geochemical and mineralogical relationships and to determine how geothermal systems may respond given 'spontaneous' injection of $scCO_2$ into a granitic reservoir. This study differs from similar studies by virtue of the use of a more realistic geothermal groundwater composition. Distilled waters were used in previous relevant studies (Suto et al., 2007; Liu et al., 2003; Lin et al., 2008).

APPROACH

Experimental Design

Simulations and experiments emulate geothermal conditions, aqueous geochemistry, and mineralogy of hydrothermal systems such as Roosevelt Hot Springs, Utah (Capuano and Cole, 1982). As pertaining to EGS with $scCO_2$ as a working fluid, experiments also emulate conditions during which reservoir groundwater has not yet been displaced by $scCO_2$ and is saturated with aqueous CO_2. These conditions may persist for months to years, and would most affect zones in proximity to injection and production pathways.

A granitic composition consisting of sub-equal portions of quartz, plagioclase feldspar, and potassium feldspar (K-feldspar) was selected for these experiments based on the composition of the majority of earth's granites (Best, 1995). Additionally, this particular granitic composition is representative of provenance for many sedimentary formations that are EGS candidates. Biotite was also included to more closely simulate a natural granite as well as to provide a source of Fe and Mg in each experimental system. Inclusion of additional accessory minerals was avoided to simplify the analysis of modeling and experimental results. Based on groundwater geochemistry at Roosevelt Hot Springs, a dominantly Na-Cl water was used in these experiments. This composition is typical of many

crystalline basement groundwaters. See below for additional details regarding reactants.

The results of three hydrothermal experiments are presented herein, including one baseline water-granite experiment, and two water-granite-$scCO_2$ experiments, each with a different initial pH. Table 1 outlines experimental conditions and parameters for each experiment. Related information is not repeated within the text. Note that during $scCO_2$ injection, the system pressure is modified to an appropriate and safe operating pressure. It then decreases to a steady state over a period of 1-2 days as CO_2 dissolves into solution. The amount of CO_2 injected in each experiment was intended to ensure aqueous CO_2 saturation for the duration of each experiment. The Duan et al. (2006) equation of state for CO_2 was utilized to calculate these target amounts of injected CO_2.

Geochemical Calculations

Equilibrium modeling was performed using Geochemist's Workbench (GWB) (Bethke and Yeakel, 2009), the b-dot ion association model, and the resident thermodynamic database thermo.com.V8.R6+.dat. The database was adjusted to include calculated equilibrium constants for the plagioclase feldspar composition used in the experiments.

Initial GWB calculations were conducted to determine a groundwater chemistry that would be as close to equilibrium as possible with the granite. This was done to minimize water-rock interaction in the hydrothermal experiments prior to CO_2 injection. GWB was also used to simulate experimental results, pre- and post-CO_2 injection.

METHODS AND MATERIALS

Experimental Apparatus

Hydrothermal experiments were conducted in rocking autoclaves (rocker bombs) and flexible Au-Ti reaction cells (Dickson cells) using established methods (Seyfried et al., 1987). Each gold cell has a volume of 220-250 cm^3 and is mated with a titanium head and exit tube. The exit tube ports directly to a metered sample valve, external to the experimental system.

The configuration of the pressure vessel and reaction cell allows for periodic sampling of either the liquid or gas phase without perturbation to the experiment. Maximum fluctuations for temperature and pressure were approximately ±2.4 °C and ±1.0 MPa, respectively (Table 1). Aqueous samples were collected approximately every 1, 2, 5, 14, and 28 days for each stage of an experiment (pre- or post-injection). The initial water, quenched water, un-reacted minerals, and reacted minerals were also collected for analysis.

Analytical Methods

Aqueous samples were analyzed for major cations and anions, trace metals, and pH. Multi-phase aqueous/gas samples were also analyzed for total carbon as CO_2. In addition, mineral reactants were analyzed before and after experimentation to identify resulting dissolution and precipitation features.

Experimental samples were filtered via porous titanium at the base of the titanium exit tube. Initial and quenched brine samples were filtered manually using Millipore 45μm filters. Samples for major cations were diluted approximately 10 times and acidified with trace-metal-grade nitric acid to a pH of 2. Anion and cation samples were refrigerated as soon after sampling as practicably possible.

Major cation and anion concentrations were determined by inductively-coupled plasma optical emission spectroscopy (ICP-OES) and ion chromatography, respectively. Trace metal concentrations were determined by inductively-coupled plasma mass spectrometry (ICP-MS). Bench pH was measured using an Orion pH meter and Ross microelectrode.

Table 1: Experimental conditions and parameters for hydrothermal experiments.

Experiment	Water + Granite	Moderate pH Water + Granite + $scCO_2$	Low pH Water + Granite + $scCO_2$
Initial pH	5.6	5.7	3.9
Temperature (°C)	250.1 ± 0.8	250.2 ± 0.9	250.0 ± 2.4
Pressure (MPa), Prior to $scCO_2$ injection	25.3 ± 0.7	25.0 ± 0.7	25.2 ± 1.0
Pressure (MPa), After $scCO_2$ injection	--	30.7 ± 0.9	44.8 ± 0.9
Amount of scCO2 injected (g)	--	19.7	20.7
Initial Water/Rock Ratio	19.4	20.0	19.0
Water-Rock Reaction Time (hours/days)	1024/42.7	700/29.2	674/28.1
Water-Rock-scCO2 Reaction Time (hours/days)	--	1027/42.8	1121/46.7

Total inorganic carbon, as CO_2, was analyzed by coulometric titration (Huffmann, 1977). Immediately after sample collection in a gas-tight syringe, multi-phase aqueous/gas samples were injected into the coulometer system. Results are representative of total aqueous carbon at in-situ conditions. The de-gassed samples collected for pH measurement were also analyzed for total carbon to facilitate back-calculation of in-situ pH at experimental conditions.

Minerals and mineral digests were reviewed using a combination of optical microscopy, X-ray diffraction (XRD), ICP-OES, ICP-MS, electron microprobe, high-resolution field emission scanning electron microscopy (FE-SEM), and energy dispersive spectra (EDS).

Experimental Reactants

Research-grade mineral separates were used as solid reactants in these experiments and consisted of 75% powder (<45 um) and 25% chip (0.1-0.7 cm). Quartz (Qtz), K-feldspar (Kspr), oligoclase (Olg), and biotite (Bio) mineral separates were analyzed for major and minor trace element concentrations after acid digestion by ICP-OES and ICP-MS (Table 2).

Table 2: Weight % oxide compositions of reactant minerals, as analyzed by ICP-OES and ICP-MS. 'ND' indicates concentrations below method detection limit.

Component	Qtz	Olg	Kspr	Bio
P_2O_5	ND	ND	ND	ND
MnO	ND	0.01	0.001	1.03
Fe_2O_3	0.08	0.12	0.19	22.84
MgO	ND	ND	ND	13.78
SiO_2	97.79	64.29	62.48	36.17
Al_2O_3	0.59	24.47	18.92	11.56
CaO	ND	5.23	0.22	0.10
TiO_2	0.03	0.02	0.01	2.50
Na_2O	ND	8.36	2.35	0.60
K_2O	ND	0.71	12.60	8.93
Total	98.48	103.37	96.86	97.50

Oligoclase and biotite chips were also analyzed for major element chemistry by electron microprobe (Table 3). Results indicate oligoclase is not chemically zoned.

Approximately sub-equal proportions of quartz, perthitic K-feldspar (~25 wt% albite and 75 wt% K-feldspar), oligoclase (An_{23}), and 4 wt% Fe-rich biotite were included in each experiment (Table 4). The use of mineral chips allows recovery for post-experimental examination of textures, while use of powder enhances reactivity and kinetic rates.

Table 3: Average weight % oxide compositions of oligoclase and biotite, as analyzed by electron microprobe.

Component	Olg	Std. Dev.	Bio	Std. Dev.
F	--	--	2.57	.13
Cl	--	--	.04	.02
SiO_2	61.83	0.25	38.21	1.02
FeO	--	--	17.65	0.39
Fe_2O_3	0.04	0.02	--	--
Na_2O	8.67	0.09	0.43	0.16
Al_2O_3	24.25	0.21	11.33	0.16
K_2O	0.50	0.09	9.37	0.29
MnO	--	--	0.87	0.07
MgO	--	--	13.82	0.31
CaO	4.65	0.06	0.01	0.01
TiO_2	--	--	2.12	0.17
Cr_2O_3	--	--	0.02	0.02
Total	99.94	--	96.44	--

Table 4: Mineral proportions used in each experiment.

	Qtz	Olg	Kspr	Bio
% Chip	8	8	8	1
% Powder	24	24	24	3
% Total	32	32	32	4

The synthetic groundwater (I ≅ 0.1 molal) was prepared using research-grade salts and solutions and contained molal quantities of Na, Cl, and HCO_3 and millimolal quantities of K, SiO_2, SO_4, Ca, Al, and Mg (Table 5).

Table 5: Water chemistry of synthetic groundwater, analyzed prior to use in each experiment. 'ND' indicates concentrations below method detection limit.

Parameter (mmol/kg)	Water + Granite	Moderate pH Water + Granite + $scCO_2$	Low pH Water + Granite + $scCO_2$
pH	5.6	5.7	3.9
F	0.011	0.013	0.001
Cl	161.2	149.5	134.7
SO_4	0.8	0.7	0.7
SiO_2(aq)	3.4	3.6	3.6
Fe	ND	ND	ND
Mg	0.8	0.7	0.8
Ca	1.0	1.4	0.7
Na	130.0	122.6	135.0
K	8.8	8.9	9.4
Mn	0.0001	0.0001	0.0003
Al	0.002	0.002	ND
ΣCO_2	ND(<0.1)	0.1	ND(<0.1)
Charge Balance	-13.2%	-10.7%	7.5%

EXPERIMENTAL RESULTS

XRD Analysis

Whole rock and clay fraction XRD analysis was conducted using powders from unreacted and reacted mineral sets. For each experiment, whole rock results exhibit discernible diffractogram patterns for initial reactant minerals only (Qtz, Olg, Kspr, Bio). This includes review of a stacked and normalized pattern representing results from 10 repeated analyses for one of the experiments (moderate pH water + granite + $scCO_2$). Clay fraction diffractogram patterns, however, do indicate contrasting mineralogical changes between samples (Figure 1).

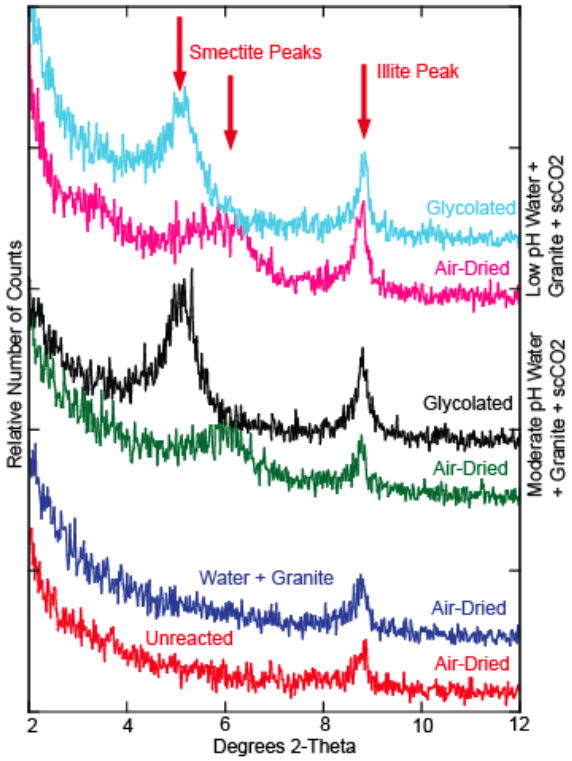

Figure 1: Clay fraction XRD patterns exhibiting illite peaks to right, and air-dried and glycolated smectite peaks on left. Results show occurrence of illite in all experiments and of expanding smectite clay in experiments injected with $scCO_2$.

XRD results for unreacted minerals and mineral powders from the water + granite experiment indicate the presence of illite clays. Of these two mineral sets, illite was only observed on mineral surfaces from the water + granite experiment, suggesting an increased presence of the clay after experimentation. XRD results also suggest relatively more illite is present in reaction products from both of the $scCO_2$ experiments. Diffractogram peaks and differences between air-dried and glycolated patterns also indicate the presence of an expanding smectite clay in the experiments injected with $scCO_2$.

Optical and SEM Analysis

Mineral dissolution and precipitation processes were reviewed and interpreted using optical microscopy, FE-SEM, and SEM-EDS. Textures of unreacted mineral fragments as compared to reacted mineral fragments suggest some dissolution of feldspar minerals within the water + granite experiment with increasing amounts of dissolution within both $scCO_2$ experiments. Mineral precipitation is also observed for all three experiments.

Three precipitates were observed in the water + granite experiment, including an abundant 'petal-forming' Mg-Fe-rich aluminosilicate (Figure 2.a), a sparse needle-forming aluminosilicate (kaolin?) (Figure 2.b), and one example of hummocky silica (amorphous?). The Mg-Fe-rich aluminosilicate also contains varying amounts of K, Ca, and Na, and appears to be zoned in reflected light, with variations from green to blue. The aluminosilicate and Mg-Fe-rich aluminosilicates are also observed in both $scCO_2$ experiments. Based on paired SEM and XRD data, we interpret the Mg-Fe-rich aluminosilicate to be an illite.

Both $scCO_2$ experiment minerals also include well-formed Fe-rich aluminosilicate rosettes (Figure 2.c). Rosettes also contain significant Mg and minor Ca, and appear blue-green in reflected light. Paired with other SEM observations and XRD data, we interpret this mineral to be a smectite. The low pH water + granite + $scCO_2$ experiment contains one additional phase of interest: euhedral scheelite ($CaWO_4$) (Figure 2.d). Scheelite was identified based on SEM-EDS data, crystal form, and optical color (rusty orange). The source of W is unknown and additional analyses are underway to understand its origin. This sample also contains very small anhedral and euhedral crystals of Au. Review is also underway to determine whether Au is a reaction product from the Au reaction cell or a contaminant from the sample coating process.

Aqueous Geochemical Analysis

Relevant major anion (Cl, SO_4, and ΣCO_2) and cation ($SiO_{2(aq)}$, Na, Ca, Na, K, Mg, and Al) data are included in Figures 3.a and 3.b for the moderate pH water- and low pH water + granite + $scCO_2$ experiments, respectively. Fe concentrations are not shown because values are below method detection limits. The time at which $scCO_2$ is injected into each system is noted on each figure. A similar plot is not provided for the baseline water + granite experiment

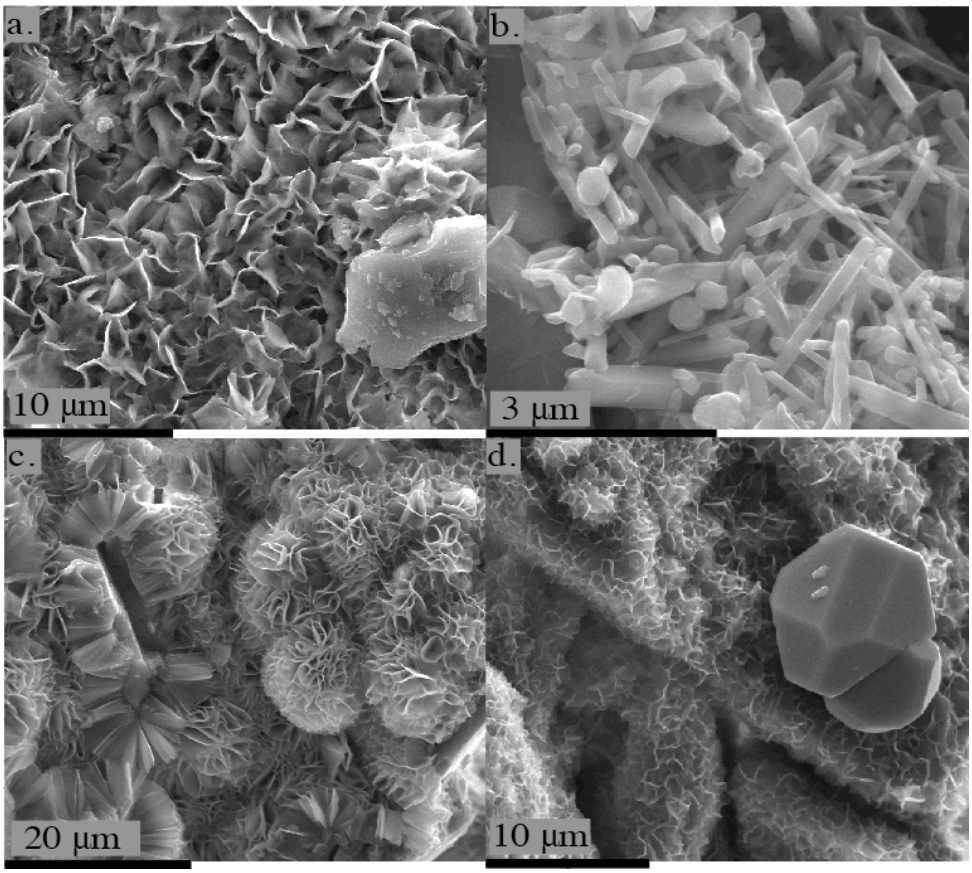

Figure 2: Representative mineral growth observed by SEM: a) Illite petals observed in all experiments; b) Needle-forming aluminosilicate observed in all experiments (kaolinite?); c) Smectite rosettes observed in scCO2 experiments only; d) Euhedral scheelite crystals observed in low pH scCO2 experiment only.

since the data mimic those trends seen in the $scCO_2$ experiments, prior to $scCO_2$ injection.

In both experiments, pre-injection trends show relatively constant concentrations of Cl, Na, SO_4, and ΣCO_2, increasing concentrations of SiO_2, K, and Al, and decreasing concentrations of Mg. The concentrations for each analyte approaches steady state prior to CO2 injection. Trends for Ca increase and then appear to decrease over time.

Post-injection trends show relatively constant concentrations of Cl, Na, and K. Concentrations of Ca, SO_4, and Al appear to decrease in both experiments during the first 5 days after injection of CO_2 while concentrations of Mg and ΣCO_2 increase over the same period of time. Post-injection concentrations of SiO_2 gradually decrease over time. Not all analytes establish a steady-state concentration prior to termination of each experiment, including SiO_2, Mg, SO_4, Al, and Ca in the moderate pH experiment and SiO_2, Mg, and Al in the low pH experiment.

When an experiment is cooled, depressurized, and the contents processed, 'quench' samples are collected to determine possible dissolution or precipitation effects caused by the quench process. A comparison of aqueous quench and pre-quench (i.e., experimental) data indicate similar concentrations of Na, Cl, K, Mg, and Al for both experiments. Ca and SO_4 quench values, however, are higher than pre-quench values, suggesting possible dissolution of a calcium sulfate phase. SiO_2 quench values are lower than pre-quench values in the moderate pH experiment, suggesting possible silica precipitation.

Results for bench pH measurements and in-situ pH calculations are also shown in Figure 3. In general, in-situ values are higher than bench values prior to $scCO_2$ injection, at which point in-situ pH values drop below bench pH values.

GEOCHEMICAL MODELING RESULTS

Preliminary forward equilibrium models indicate that pre-injection reactions will likely include feldspar alteration to clay minerals and/or low-temperature zeolites. Post-CO_2 injection calculations suggest

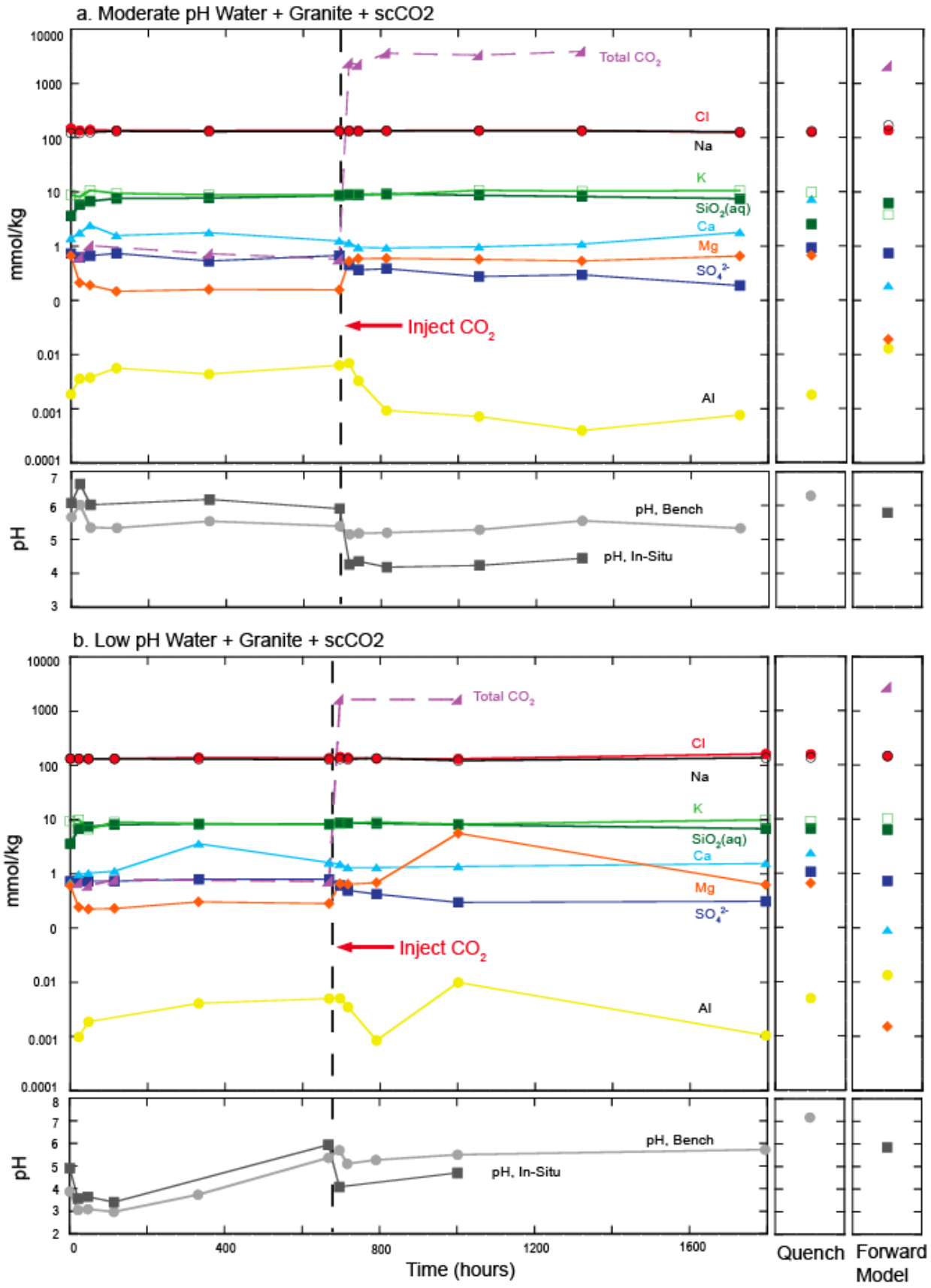

Figure 3: Major cation and anion data for a) moderate pH water + granite + scCO2 experiment and b) low pH water + granite + scCO2 experiment. Quench and forward model data are also shown at far right.

carbonates may precipitate at the expense of Ca, Mg, and Fe silicates.

Major cation and anion predictions for the $scCO_2$ experiments are shown on the right-hand side of Figure 3. Both experiments exhibit good correlation for Na and Cl, and good to fair correlation for K, SiO_2, and SO_4 concentrations between model and experimental results. Correlation is poor for pH, Mg, Ca, and Al concentrations; substantially lower values for Mg and Ca and higher values for pH and Al are predicted than are observed in experimental results.

Calculated and experimental ΣCO_2 values for the low pH experiment suggest CO_2 saturation was achieved in the experimental system. However, preliminary ΣCO_2 calculations for the moderate pH experiment are lower than experimental results, suggesting that the experiment was not saturated with respect to aqueous CO_2. This may not be accurate based on the CO_2 extraction volumes and concentrations observed during each sample event. Accordingly, CO_2 equations of state are currently under review to determine the cause for discrepancy.

DICUSSION

Clay Formation

XRD and SEM data together verify that illite formed in all experiments, and that smectite formed in response to injection of $scCO_2$. Decreasing aqueous Mg concentrations in the experiments also supports formation of Mg-Fe-rich illite during the first five days of each experiment. Increasing Mg concentrations during the first two days after $scCO_2$ injection may also signal a shift in stability from Mg-Fe-rich illite to Fe-rich smectite. (Aqueous Fe values are below method detection limits.) No textural observations link possible dissolution of biotite and/or illite to contribution of Fe towards Fe-rich smectite precipitation. Preliminary forward equilibrium model results identify smectite as a possible precipitate in pre-injection systems, but no clays are identified as likely precipitants in post-injection systems.

Clay formation of any type could affect permeability and porosity of EGS. Of particular concern may be the possible precipitation of expanding clays as a result of $scCO_2$ injection. A review of the thermodynamic processes involved in the experimental clay formation is underway.

In addition to applicability to EGS, this work may also add to the ongoing debate about hydrothermal clay formation mechanisms. Hydrothermal clay formation is thought by some to mimic that of diagenetic clay formation whereby smectite is a precursor to illite, with the conversion taking place due to increasing temperature (e.g., Inoue, 1995). To others (e.g., Bethke et al., 1986), hydrothermal clay formation can proceed via direct precipitation from solution. This debate also ties into field observations that associate smectite and intermixed smectite/illite with lower temperature regimes (<~200°C) and illite with higher temperature regimes (starting at ~200°C) (Inoue, 1995; Henley et al., 1984). Present experimental work is conducted at a steady temperature of 250°C. Therefore, it is proposed that the stable clay during pre-injection versus post-injection may relate to pH or ΣCO_2 contents during experimentation; on injection of $scCO_2$, it appears that smectite is the more stable phase and that it precipitates directly from solution. We observed no textural evidence indicating mixed or prograde reactions between illite/smectite clays. Further investigation is underway to understand how ΣCO_2 relates to silicate stability (i.e., Giggenbach, 1981).

Carbonate Formation

Preliminary equilibrium models predict carbonate formation upon injection of $scCO_2$ into the experimental systems. No carbonates were observed in any of the presented experiments. This is not an uncommon result as compared with recent granite + liquid water + CO_2 experimental research (Lin et al., 2008; Suto et al., 2007; Liu et al., 2003). Depending on the goal of any given EGS, this result may have implications for projects intended to sequester carbon in a granitic reservoir.

As noted above, once the review of the CO_2 equation of state is completed and the geochemical database modified accordingly, a comparison of predicted vs. experimental results will be conducted. A careful look at silica and carbon activities and buffering capacities may be needed to resolve the discrepancy between modeled and experimental systems.

Scheelite Formation

The significance of scheelite formation in the low pH water + granite + $scCO_2$ experiment is unknown, as is the source for W. Scheelite is found naturally in granitic hydrothermal systems, so it is not unreasonable that it formed in the given experimental system. Homogenization temperatures of fluid inclusions in scheelite range from 200-400 °C, with the most occurrences ranging from 200-300 °C. Compiled data also indicate an increased occurrence of scheelite with fluids of high CO_2 content (Naumov et al., 2011). These parameters appear to be in line with the given experimental system.

CONCLUSIONS

A baseline understanding of reactions involving a multi-component groundwater, a granite, and $scCO_2$ has been established. Major implications of this study include 1) possible formation of expanding clays after injection of scCO2 into a granite-hosted geothermal system at typical conditions of 250 °C and 250-450 bars and 2) a lack of carbonate formation as may be desired for carbon sequestration. Since EGS will likely require stimulation of a reservoir by fracturing, additional experiments will add typical vein minerals, e.g. epidote, chlorite, and/or calcite.

ACKNOWLEDGEMENTS

This project is supported by DOE grant DE – EE0002766 to Lu, Kaszuba, McPherson, Moore, et al., cost share from the UW School of Energy Resources (SER), and an Encana Corporation graduate assistantship to Lo Ré. The experimental hydrothermal laboratory was constructed with funding from SER. Peter Lichtner (Los Alamos National Laboratory) is acknowledged for geochemical modeling assistance as is the Laboratory for Environmental and Geological Studies (LEGS) for conducting ICP and ion chromatography aqueous geochemistry.

REFERENCES

Best, M. (1995), *Igneous and Metamorphic Petrology*, Blackwell Science, Cambridge, MA: 630p.

Bethke, C., Vergo, N., Altaner, S. (1986), "Pathways of smectite illitization," *Clays and Clay Minerals*, **34**, 135-135.

Bethke, C. and Yeakel, S. (2009), *The Geochemist's Workbench Release 8.0: Reaction Modeling Guide*, University of Illinois, Champaign, Illinois, 84p.

Brown, D. (2000), "A hot dry rock geothermal energy concept utilizing supercritical CO_2 instead of water," *Proceedings of the Twenty-Fifth Workshop on Geothermal Reservoir Engineering*, Stanford University: 233-238.

Capuano, R. and Cole, D. (1982), "Fluid-mineral equilibria in a hydrothermal system, Roosevelt Hot Springs, Utah," *Geochemica et Cosmochimica Acta*, **46(8)**: 11353-1364.

Duan, Z., Sun, R., Zhu, C., and Chou, I. (2006), "An improved model for the calculation of CO_2 solubility in aqueous solutions containing Na^+, K^+, Ca^{2+}, Mg^{2+}, Cl^-, and SO_4^{2-}," *Marine Chemistry*, **98**, 131-139.

Giggenbach, W. (1981), "Mass transfer in hydrothermal alteration systems – A conceptual approach," *Geochimica et Cosmochimica Acta*, **48**, 2693-2711.

Henley, R., Truesdell, A., Barton, P. Jr., and Whitney, J. (1984), "Fluid-mineral equilibria in hydrothermal systems," *Reviews in Economic Geology*, **1**, J. Robertson, Society of Economic Geologists, 65-82.

Huffmann, E. (1977), "Performance of a new automatic carbon dioxide coulometer," *Microchemical Journal*, **22(4)**, 567-573.

Inoue, A, (1995), "Formation of clay minerals in hydrothermal environments", *Origin and Mineralogy of Clays: Clays and the Environment*, B. Velde, Springer-Verlag, New York, 245-329.

Naumov, V., Dorofeev, V., and Mironova, O. (2011), "Physicochemical parameters of the formation of hydrothermal deposits: A fluid inclusion study: I. Tin and tungsten deposits," *Geochemistry International*, **49(10)**, 1002-1021.

Lin, H., Fujii, T., Takisawa, R., Takahashi, T., Hashida, T. (2008), "Experimental evaluation of interactions in supercritical CO_2/water/rock minerals system under geologic CO_2 sequestration conditions," *Journal of Materials Science*, **43(7)** 2307-2315.

Liu, L., Suto, Y., Bignall, G., Yamasaki, N., Hashida, T. (2003), "CO_2 injection to granite and sandstone in experimental rock/hot water systems," *Energy Conversion and Management*, **44(9)**, 1399-1410.

Pruess, K. (2006), "Enhanced geothermal systems (EGS) using CO_2 as a working fluid – A novel approach for generating renewable energy with simultaneous sequestration of carbon," *Geothermics*, **35(4)**, 351-367.

Seyfried, W., Janecky D., and Berndt, M. (1987), "Rocking autoclaves for hydrothermal experiments II: The flexible reaction-cell system," *Hydrothermal Experimental Techniques*, G. Ulmer and H. Barnes, New York, John Wiley & Sons: 216-239.

Suto, Y., Liu, L., Yamasaki, N., Hashida, T. (2007), "Initial behavior of granite in response to injection of CO_2-saturated fluid," *Applied Geochemistry*, **22(1)**, 202-218.